Ablation study in the capillary discharge of an electrothermal gun

Michael Keidar[a] and Iain D. Boyd
Department of Aerospace Engineering, University of Michigan, Ann Arbor, Michigan 48109-2140

(Received 26 May 2005; accepted 23 January 2006; published online 1 March 2006)

In this paper, we study the ablation phenomena associated with the operation of a capillary discharge for an electrothermal gun. Electrothermal-chemical (ETC) guns are used for enhancement of ignition and combustion of an energetic propellant. One of the major components of the ETC system is a plasma source based on a capillary discharge. In this paper, a model of the capillary discharge is developed. In this model, primary attention is paid to the ablation phenomenon. Different characteristic subregions near the ablated surface, namely, a space-charge sheath, a Knudsen layer, and a hydrodynamic layer, are considered. In this formulation, the ablation rate is determined by the parameters at the edge of the Knudsen layer. The kinetic approach is used to determine the parameters at the interface between the kinetic Knudsen layer and the hydrodynamic layer. Coupling the solution of the nonequilibrium Knudsen layer with the hydrodynamic layer provides a self-consistent solution for the ablation rate. According to the model predictions, the peak electron temperature is about 1.4 eV, the polyethylene surface temperature is about 700 K, and the pressure is about 10 MPa. It is found that the ablation rate increases with the capillary length. The ablated mass and the predicted total pressure agree with previous experimental observations. © *2006 American Institute of Physics*. [DOI: 10.1063/1.2174111]

I. INTRODUCTION

Electrothermal-chemical (ETC) guns are designed to introduce electrical energy into the chamber of a conventional chemical gun system.[1] An ETC gun has the potential to improve the performance of conventional guns by enhancing the ignition and combustion characteristics of propellants. One of the significant advantages of the ETC system is a smaller ignition delay time as compared with conventional igniters. Typically, ETC ignition delay is of the order of 1–2 ms, while advanced conventional igniters have been shown to exhibit 6–8 ms ignition delay.[1] An ETC system has two components, namely, a plasma source and a chemical propellant system. In this sytem, the propellant is usually ignited with plasma introduced by a jet from a capillary discharge or by an arc from an exploding wire inside the propellant charge.[1–3] Several plasma properties are important for this application. The temperature of the plasma is about 10 000 K. Significant radiation from the plasma leads to photochemical changes within the propellant surface and in-depth structure. The presence of various ion and neutral species may lead to chemical reaction at the propellant surface. In addition, the highly directed velocity of the plasma jet affects the heat transfer. All of the above plasma-propellant interactions are dependent on the plasma properties that are determined by the plasma source. Therefore, accurate prediction of plasma properties from the capillary discharge is important for understanding plasma-propellant interactions. The main physical processes occur in the capillary in a similar way to an ablation-controlled discharge. Rapid heating of a thin dielectric surface layer leads to the decomposition of the material of the wall. As a result of heating, decomposition, and partial ionization of the decomposition products, the total number of particles increases in the cavity, thus leading to the formation of a dense plasma outflow from the capillary.

Significant efforts have been applied to model the ablation-controlled discharge, which is commonly used as a plasma source for ETC.[4–7] The problem of the ablation-controlled discharge also has a more general interest since it can be used for various applications such as electric fuses, circuit breakers, plasma thrusters, soft x-ray, and extreme ultraviolet sources.[8–12] In these devices, the discharge energy is principally dissipated by the ablation of the wall material, which then forms the main component of the discharge plasma.

Some initial theoretical models aimed to analyze available experimental data[13] and build a phenomenological description of the ablation processes. Later, more sophisticated steady state[14] and unsteady theoretical models[5,15–19] were proposed to describe capillary discharges for an electrothermal gun. However, these models are based on some assumptions about the ablation rate. In most models, the ablation rate is determined somewhat arbitrarily or adjusted to fit the measured total ablated mass. Previous models used mainly the gray-body radiation model with gray factor f to adjust the ablation rate. The gray factor is chosen to agree with experimentally measured total ablated mass.[5–8] Zoler and Alimi[6] proposed to decrease the arbitrariness of the choice of f by considering radiation. It was, however shown recently that material ablation into the discharge plasma is a rather complicated phenomenon.[20,21] For instance, the same ablation rate can correspond to very different discharge conditions. A self-consistent model of the capillary discharge that takes into account ablation kinetics with application to a plasma thruster was developed recently.[22] In this approach, the ablation of the propellant in contact with a high-pressure discharge plasma was modeled using the direct simulation

[a]Electronic mail: keidar@umich.edu

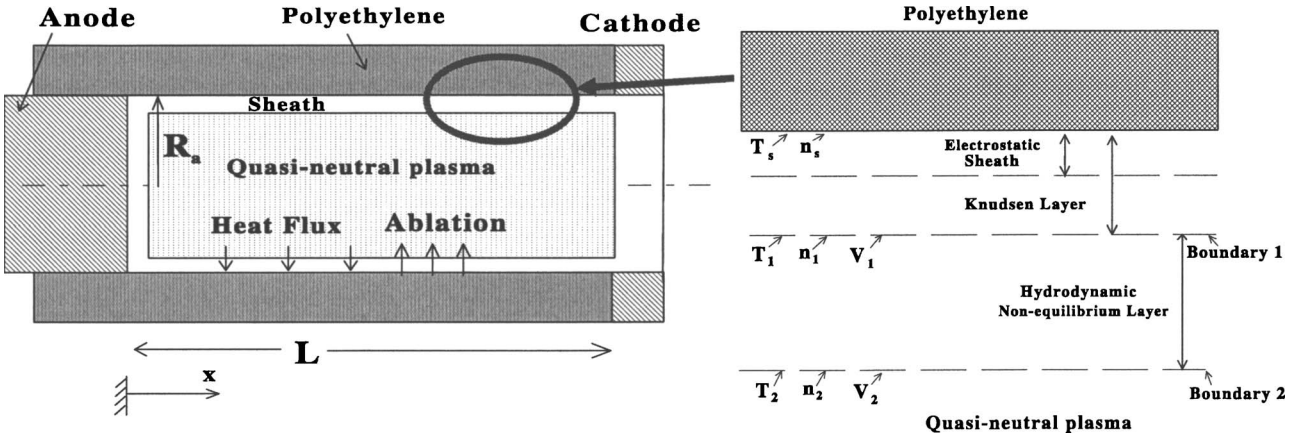

FIG. 1. Schematic of the problem geometry (not to scale) and multilayer structure near the ablated surface.

Monte Carlo (DSMC) particle method[23] and an analytical kinetic approach based on the bimodal distribution function approximation.[20] Effects related to the presence of the plasma in the vicinity of ablated materials were included. The model is based on a kinetic description of the Knudsen layer and a hydrodynamic description of the collision-dominated plasma region. One of the significant results of this model is that a substantial flux of the atoms and ions returns to the surface from the plasma depending on the plasma conditions.[20–22]

In this paper, we present a capillary model for an ETC that includes self-consistent consideration of the ablation phenomena. The backflux of particle leads to the formation of a thin layer over the dielectric surface that, in turn, is evaporated. The balance between evaporation and condensation in addition to the mass, momentum, and energy conservation in the Knudsen layer determines the total ablation rate. We describe the ablation model and the coupling of this model with a plasma capillary discharge model by considering a specific example of a polyethylene capillary for an ETC. The discharge model including consideration of the quasineutral plasma and sheath, polyethylene ablation, and heat conduction is described in Sec. II. Results of the calculation are presented in Sec. III followed by the concluding remarks (Sec. IV).

II. THE DISCHARGE MODEL

In this section we describe the model for the plasma generation processes (ablation, heating, radiation, ionization, etc.) and plasma acceleration along a capillary of a pulsed electrical discharge. Figure 1 shows some characteristic regions in the interface between the discharge plasma and the dielectric wall such as an electrical sheath near the dielectric, the Knudsen and hydrodynamic layers, and a quasineutral plasma. Different kinetic and hydrodynamic phenomena determine the main features of the plasma flow including Joule heating, radiative and convective heat transfers to the dielectric, and electrothermal acceleration of the plasma up to the sound speed at the cavity exit. Below we discuss models of the different regions and the full system of equations. The central region is the quasineutral plasma that occupies almost the entire capillary since typically the transition region scale length is much smaller than the capillary radius. The plasma region is separated from the dielectric surface by the vapor layers (Knudsen layer and hydrodynamic layer). Finally, the plasma-wall transition region includes the electrostatic sheath attached to the wall. We start from considering the quasineutral plasma region.

A. Quasineutral plasma

The basic set of equations describing the evolution of the plasma is similar to that previously developed for the ablative discharge in the pulsed plasma thruster.[22] The plasma region extends over almost the entire capillary radius R_a, since all considered boundary layers are very thin.[22] The plasma is heated due to electric current flowing through the capillary. The energy transfer from the plasma column to the capillary wall consists of the heat transfer by particle fluxes and radiation. Energy is absorbed by the capillary walls and dissipated by heat conductivity and material evaporation. Ablated flux builds the vapor layer in the vicinity of the wall. Previous models of the ablation-controlled discharge show that the axial pressure and velocity variations are much greater than those in the radial direction.[14,24] Therefore we will assume that all parameters vary in the axial direction x as shown in Fig. 1, but are uniform in the radial direction. Under the considered conditions the mass, momentum, and energy conservation equations have the following forms:

$$A\left(\frac{\partial \rho}{\partial t}+\frac{\partial \rho V}{\partial x}\right)=2\pi R_a \Gamma(t,x), \tag{1}$$

$$\rho\left(\frac{\partial V}{\partial t}+V\frac{\partial V}{\partial x}\right)=-\frac{\partial P}{\partial x}, \tag{2}$$

$$\rho\left(\frac{\partial \varepsilon}{\partial t}+V\frac{\partial \varepsilon}{\partial x}\right)=-P\frac{\partial V}{\partial x}+Q_j-Q_r-Q_F, \tag{3}$$

where $\varepsilon=(3/2)(T_p/m)+(V^2/2)$, T_p is the plasma temperature, Γ is the ablation rate, R_a is the capillary radius, A is the capillary cross section, ρ is the density, V is the velocity, P is the pressure, and Q_j is the Joule heat. The Joule heat term is equal to $Q_j=j^2/\sigma$, where j is the current density and σ is the electrical conductivity. The electrical conductivity is deter-

mined by electron collisions with ions and neutral atoms and can be expressed as $\sigma = n_e e^2/m_e(\nu_{ei}+\nu_{en})$, where ν_{ei} is the electron-ion collision frequency and ν_{en} is the electron-neutral collision frequency. The radiation energy flux Q_r includes the radiation for a continuum spectrum based on a theoretical model.[25] According to Ref. 26, the radiation in continuum from a carbon plasma in the considered parameter range provides the main contribution. In addition, a blackbody radiation from the plasma will be considered and compared with other energy sources and sinks. The particle convection flux Q_F includes energy associated with electron and ion fluxes to the dielectric wall that leads to plasma cooling (will be discussed in more detail below). Our estimations and previous calculations show that the electron temperature varies only slightly with axial position and therefore we performed the calculation assuming $\partial T_p/\partial x = 0$.

1. Heat conduction

Radiation and convection heat fluxes from the plasma to the cavity wall (see Fig. 1) determine the thermal regime of the capillary walls. The temperature inside the dielectric can be calculated from the heat transfer equation as follows:

$$\frac{\partial T}{\partial t} = a\frac{\partial^2 T}{\partial r^2}, \tag{4}$$

where a is the thermal diffusivity. This is the one-dimensional equation in the radial direction. This assumption can be made since the heat layer thickness near the surface is smaller than the polyethylene cylinder curvature R_a and also less than the characteristic length of plasma parameter changes in the axial direction. Also we assume that the electron temperature variation in the axial direction is small as will be shown later in Sec. III. In order to solve this equation, boundary and initial conditions must be specified:[22]

$$\begin{aligned} &-\lambda\,\partial T/\partial r(r=R_a) = q(t) - \Delta H\cdot\Gamma - C_p(T_s - T_o)\Gamma, \\ &\lambda\,\partial T/\partial r(r=\infty) = 0 \\ &T(t=0) = T_o, \end{aligned} \tag{5}$$

where $r=R_a$ corresponds to the inner dielectric surface, ΔH is the ablation heat, Γ is the rate of polyethylene ablation per unit area, T_o is the initial room temperature, $q(t)$ is the density of the heat flux, consisting of the radiative and particle convection fluxes (determined by an expression similar to that used in Ref. 22), and T_s is the surface temperature. The solution of this equation is considered for two limiting cases of substantial and small ablation rates very similar to that described in Ref. 22.

2. Plasma composition

Having calculated the plasma density and electron temperature [Eqs. (1)–(3)] one can calculate the chemical plasma composition considering local thermodynamic equilibrium (LTE) in the way described previously.[22,27,28] In the considered range of electron temperature (1–2 eV) and plasma density (10^{24}–10^{26} m^{-3}) we will assume that polyatomic molecules C_2H_4 fully dissociate and we will start our consideration from the point when we have a gas containing atoms of C and H. Under such conditions, plasmas are expected to be in LTE, which means that the plasma composition is determined by the local state of the plasma. The plasma composition is determined by the Saha equations for each species.[22] The distribution of the atoms, multiply ionized ions, and electrons obeys the corresponding Saha equation. Knowing the plasma pressure and temperature, ionization potential, and partition functions for z-fold ionization processes allows the calculation of the atom and ion species density. Saha equations should be supplemented by the conservation of nuclei and quasineutrality in order to calculate the plasma composition.

3. Weakly nonideality corrections

In the considered range of parameters it is expected that the plasma is in LTE as discussed before. However, the standard LTE model is only accurate for the calculation of the composition of an ideal plasma.[22] However, a plasma may depart from the ideal state under the considered high-density conditions. Due to plasma nonideality effects, one should consider corrections to the ionization energies, partition functions, and plasma pressure.[29] While the Saha equilibrium equations that were described above can sufficiently describe the plasma composition for ideal plasmas, nonideality corrections should be taken into account. The degree of nonideality can be estimated as follows:[30]

$$\zeta = \frac{e^2(n_i + n_e)^{1/3}}{4\pi\varepsilon_o T_p}. \tag{6}$$

Accordingly, if $\zeta < 0.1$ the plasma can be considered ideal, and weakly nonideal if $0.1 < \zeta < 1$. In the case of a weakly nonideal plasma, corresponding corrections were derived previously.[29] The corresponding corrections for the ionization energy and plasma pressure have the following forms:

$$\Delta I_i^z = \frac{(z+1)e^2}{4\pi\varepsilon_0 R_D}, \tag{7}$$

where z is the ion charge state and R_D is the Debye radius.

$$\Delta P = \frac{1}{6}\cdot\frac{e^2}{4\pi\varepsilon_o R_D}, \tag{8}$$

taking this into account, the effective ionization energy in a high-density plasma can be expressed as follows: $I_i^z = I_{\text{ideal}}^z - \Delta I_i^z$, while the pressure can be expressed as $P = P_{\text{ideal}} - \Delta P$.

One can easily estimate the plasma nonideality parameter for typical conditions during the capillary discharge. Our estimations show that the plasma composition can be affected by nonideal effects if the heavy particle density is larger 10^{26} m^{-3} and plasma temperature is about 1 eV.

B. Polyethylene ablation model

We model the capillary wall ablation in the framework of the previously developed kinetic model.[20,21] Two different layers between the ablated surface and the plasma bulk are considered as shown in Fig. 1: (i) a kinetic nonequilibrium layer adjacent to the surface with a thickness of about one mean free path and (ii) a collision-dominated layer with ther-

mal and ionization nonequilibrium. The plasma-wall transition layer includes also an electrical sheath described below. By solving the energy, momentum, and mass conservation equations across the Knudsen layer, one can obtain the parameters (density and temperature) at the interface between the kinetic and hydrodynamic layers (boundary 1 in Fig. 1) if the velocity at this boundary V_1 is know.[20] In turn, the velocity V_1 can be determined by coupling the solution of the hydrodynamic layer and the quasineutral plasma. Solving the conservation equations in the hydrodynamic layer[21] one finds that the ablation rate has the following form:

$$\Gamma = mV_1 n_1 = mn_1 \sqrt{\frac{1}{m} \cdot \frac{(kn_2T_2 - kn_1T_1)}{[n_1 - (n_1^2/n_2)]}}. \tag{9}$$

It should be noted that Eq. (9) has a real solution if the following conditions are fulfilled:

$$kn_1T_1 > kn_2T_2 \quad \text{and} \quad n_1 > n_2, \tag{10}$$

otherwise, the solution of Eq. (9) breaks down. The backflux becomes higher than the primary flux if condition (10) fails. The backflux is controlled by pressure in the capillary, which is established as a result of a balance between the ablation and the mass losses through the capillary exit. High pressure leads to the increase of the backflux to the capillary walls. When backflux is high the deposition on the dielectric surface takes place instead of ablation. In the transient regime of the capillary operation both cases are possible and therefore we will consider both cases in the model. However, as expected (see results below), the ablation rate is positive in average. In order to take the considered effects into account, the deposition rate can be calculated as follows:

$$\Gamma = -m(kT_2/m)^{0.5} n_{C2}, \tag{11}$$

where n_{C2} is the carbon particle density at boundary 2, which is approximately $n_{C2} = \frac{1}{3} n_2$ for polyethylene. In Eq. (11), the negative sign means that material deposition occurs instead of evaporation. It is assumed that only carbon atom and carbon ion depositions take place, as the hydrogen atoms and ions will be reevaporated. This assumption is supported by previous studies of dielectric (Teflon) ablation into C–F plasmas, which indicated that the dielectric can be significantly carbonized (charred) depending on operational conditions.[31] Based on observations and simulations[31] it was concluded that the carbon char is formed as a result of the carbon flux that returned from the plasma.

The system of equations is closed if the equilibrium vapor pressure can be specified, which determines the parameters (n_s and T_s) at the dielectric surface. In the case of polyethylene, various models[32] and an experiment[33] show that the vapor pressure for polyethylene can be approximated as follows:

$$P_v = \exp\left[A \cdot \left(\frac{1}{B} - \frac{1}{T}\right)\right] \quad \text{(bar)}, \tag{12}$$

where $A = 5565.22$, $B = 453$, and T is in kelvin.

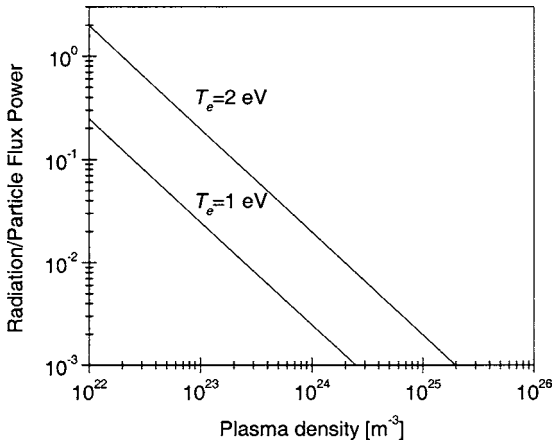

FIG. 2. Ratio of the radiation to convection power as a function of plasma density with electron temperature as a parameter.

C. Sheath

Near the dielectric surface in the capillary an electrostatic sheath is formed to maintain the steady state floating potential on the wall with respect to the plasma, i.e., zero total current to the wall. A simple estimation shows that under the typical capillary discharge conditions this sheath is unmagnetized (i.e., electron Larmor radius is much larger than the Debye length) in the self-magnetic field generated during the pulse. Typically, the thermal electron current density j_{eth} is much larger than the ion current density j_i, and therefore the steady state potential drop across the sheath is negative to maintain the total current to the wall equal to zero. This potential drop in the sheath can be calculated as follows:

$$U_d = -T_p \ln(j_{\text{eth}}/j_i). \tag{13}$$

Based on the sheath model one can calculate the total particle flux consisting of ion and electron fluxes to the wall as follows:

$$Q_f = j_i(2T_p + U_d + T_p). \tag{14}$$

III. RESULTS

In this paper we consider a specific capillary plasma source for an ETC described recently by Beyer and Pesce-Rodriguez.[34] This plasma source has a polyethylene capillary of 3 mm diameter and 35 mm length. The pulse duration is about 300 μs and the current peaks at about 2.6 kA. Electrode materials are made of carbon.

The relative contributions of the various energy fluxes to the dielectric surface are calculated depending on the plasma conditions. The calculated ratio between the radiative and convective particle flux contributions is shown in Fig. 2. One can see that the relative contribution of the particle flux prevails for typical capillary discharge conditions except in the low-density range. It will be shown below that plasma density during the main part of the discharge is larger that 10^{24} m^{-3}.

It is important to know the relative contribution of the electrode erosion. Central electrode (anode) erosion is a major concern as was discussed by Taylor.[35] Cathode erosion

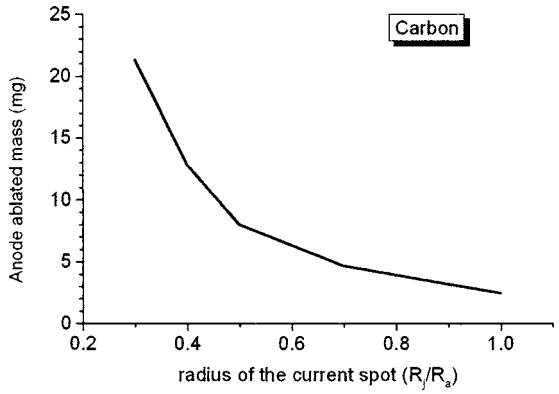

FIG. 3. Anode ablated mass as a function of radius of the current spot at the anode.

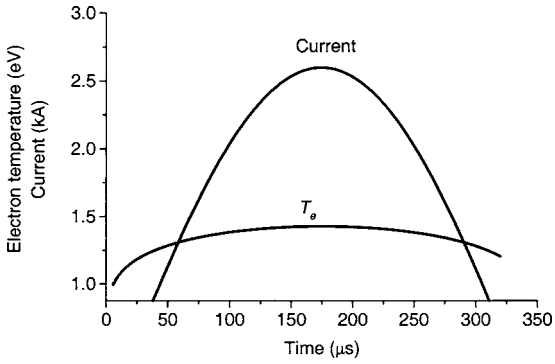

FIG. 4. Temporal variation of the electron temperature and current wave form used in the simulations.

rate depends on the electrode material and current distribution near the electrode as shown in Fig. 3. One can see that current constriction leads to a significant increase of the erosion rate with current constriction degree. However, our estimations suggest that current constriction is very small under typical capillary conditions. Therefore, according to these predictions the anode erosion mass is relatively small and typically is about 3 mg, which is only a fraction of the total ablated mass as will be shown below.

The electron temperature temporal variation during the discharge is shown in Fig. 4. For reference, the adopted experimentally measured current wave form is also shown. It can be seen that the electron temperature temporal distribution follows the current wave form. The temperature peaks at 1.4 eV and then decreases towards the end of the pulse.

Different species spatial and temporal distributions are shown in Fig. 5. All species densities peak at about 150–200 μs. One can see that the neutral density is much higher than the ion density, thus indicating that the ionization degree is small (approximately 10%–20% for the main portion of the pulse).

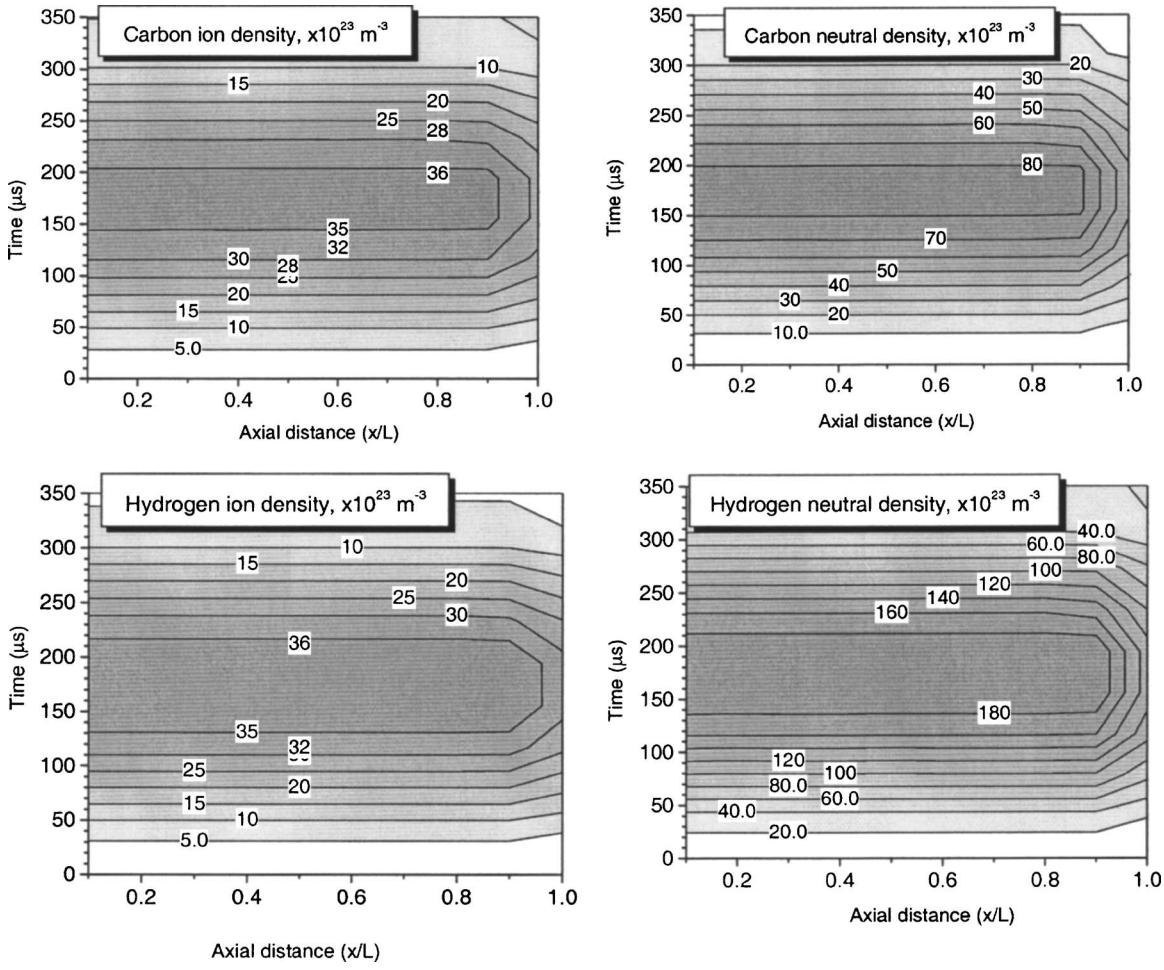

FIG. 5. Temporal and spatial variations of the chemical species during discharge pulse.

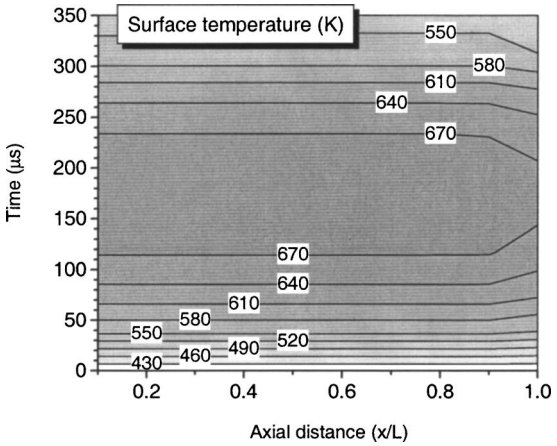

FIG. 6. Temporal and spatial variations of the polyethylene surface temperature.

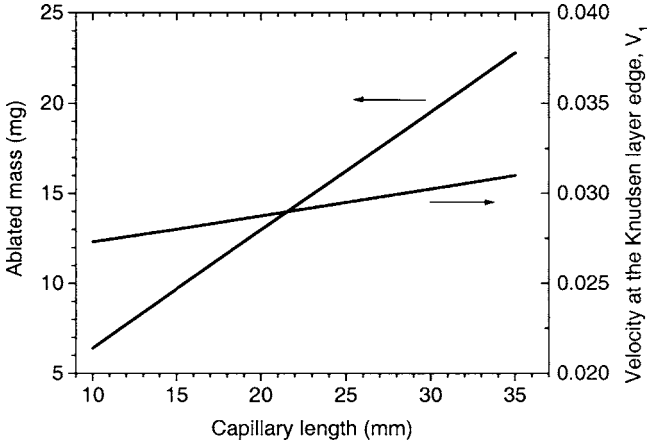

FIG. 8. Dependence of the ablated mass and velocity at the Knudsen layer edge on the capillary length.

The surface temperature distribution is shown in Fig. 6. The surface temperature sharply increases initially and peaks at about 700 K. Only a slight variation of the surface temperature along the capillary is found in accordance with previous predictions (Ref. 22).

Total pressure axial and temporal distributions are shown in Fig. 7. It can be seen that pressure peaks at about 10 MPa and then decreases towards the end of the pulse to about 1 MPa. Calculation of the pressure in the capillary from discharge current and external pressure measurements[34] suggests that the pressure in the capillary peaks at about 15 MPa, which is close to this model's predictions.

Capillary geometry determines the ablation process in the capillary by affecting the mass and energy balance. For instance, the dependence of the ablated mass on the capillary length is shown in Fig. 8. It should be noted that the total ablation mass in the case of $L=35$ mm agrees with experiment,[34] in which the total ablated mass was about 25 mg.

The average velocity at the Knudsen layer edge that determines the ablation rate is also shown in Fig. 8. One can see that this velocity is much smaller than the sound speed, thus indicating the importance of the kinetic ablation model. It is important to note that the velocity at the Knudsen layer edge shown in Fig. 8 is the average velocity during the pulse, which has a small variation with the capillary length.

Finally, the dependence of the peak pressure in the capillary on the discharge energy is shown in Fig. 9. Peak pressure increases nearly linearly with the discharge energy, indicating that the power conversion for the given capillary parameters is approximately constant.

IV. CONCLUDING REMARKS

In this paper, a model of the capillary discharge for ETC guns was developed. The most important aspect of the capillary modeling is the accurate analysis of the ablation phenomenon, which determines the plasma parameter evolution during the capillary discharge. Consistent analysis of the different characteristic regions near the ablated surface allows calculating the rate of ablation without employing the various assumptions used previously. For instance, it turns out that it is not necessary to assume the energy fraction causing the capillary wall ablation. In the case when the capillary pressure exceeds the equilibrium pressure, the negative ablation rate, i.e., material deposition on the capillary walls, is possible. The main component of the backflux is the carbon leading to surface carbonization. It should be emphasized that carbon film buildup on the polyethylene surface may lead to significant changes in the evaporation rate.

According to the model prediction, the carbon electrode ablation rate is small in comparison to the polyethylene ab-

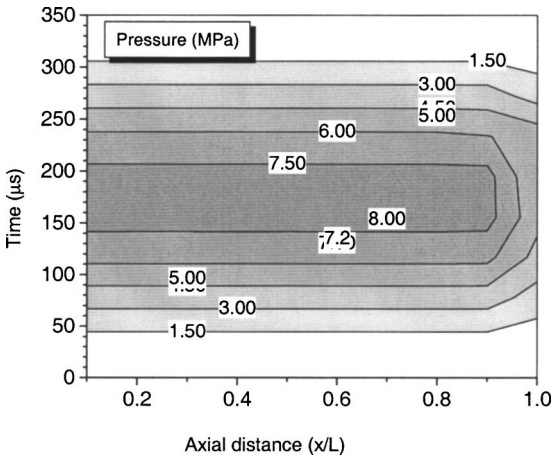

FIG. 7. Temporal and spatial variations of the pressure in the capillary.

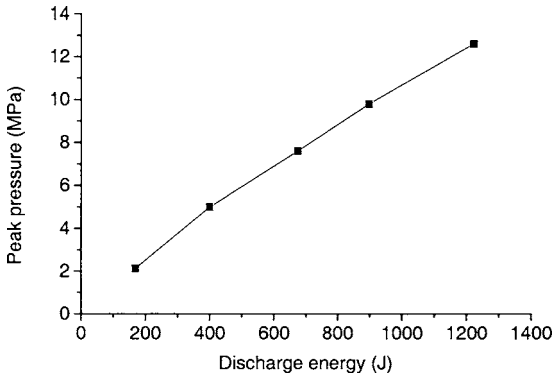

FIG. 9. Dependence of the peak pressure on the discharge energy.

lation mass. It was found that the ablated mass increases approximately linearly with the capillary length, thus indicating that capillary discharge is uniform and total pressure changes only slightly with the capillary length increase. This can be seen also from the analysis of the velocity at the Knudsen layer edge, which shows very little dependence on the capillary length.

ACKNOWLEDGMENTS

The authors gratefully acknowledge the financial support by the Army Research Office, Grant No. W911NF-04-1-0251 (Dr. David Mann is the technical manager). They also thank Dr. Richard Beyer, Dr. Michael Nusca, and Dr. Anthony Williams from the Army Research Laboratory for very useful discussions and suggestions.

[1]A. Koleczko, W. Ehrhard, S. Kelzenberg, and N. Eisenreich, Propellants, Explos., Pyrotech. **26**, 75 (2001).
[2]A. Birk, M. D. Guercio, A. Kinkennon, D. E. Kooker, and P. Kaste, Propellants, Explos., Pyrotech. **25**, 133 (2000).
[3]J. Li, T. A. Litzinger, and S. T. Thynell, J. Propul. Power, **21**, 44 (2005).
[4]D. Zoler, D. Saphier, and R. Alimi, J. Phys. D **27**, 1423 (1994).
[5]J. D. Powell and A. E. Zielenski, IEEE Trans. Magn. **29**, 591 (1993).
[6]D. Zoler and R. Alimi, J. Phys. D **28**, 1141 (1995).
[7]M. R. Zaghloul, M. A. Bourham, and J. M. Doster, J. Phys. D **34**, 772 (2000).
[8]L. Muller, J. Phys. D **26**, 1253 (1993).
[9]E. Domejean, P. Chevrier, C. Fievet, and P. Petit, J. Phys. D **30**, 2132 (1997).
[10]S. V. Kukhlevsky, J. Kaiser, O. Samek, M. Liska, and J. Erostyak, J. Phys. D **33**, 1090 (2000).
[11]D. Hong *et al.*, Rev. Sci. Instrum. **71**, 15 (2000).
[12]M. Keidar, I. D. Boyd, and I. I. Beils, IEEE Trans. Plasma Sci. **28**, 376 (2000).
[13]E. Z. Ibrahim, J. Phys. D **13**, 2045 (1980).
[14]C. B. Ruchti and L. Niemeyer, IEEE Trans. Plasma Sci. **14**, 423 (1986).
[15]R. L. Burton, B. K. Hilko, F. D. Witherspoon, and G. Jaafari, IEEE Trans. Plasma Sci. **19**, 340 (1991).
[16]D. A. Tidman, Y. C. Thio, S. A. Goldstein, and D. S. Spicer, GT Devices Technical Note No. GTD 86-7, 1986 (unpublished).
[17]A. Loeb and Z. Kaplan, IEEE Trans. Magn. **25**, 342 (1989).
[18]R. B. Mohanti, J. G. Gilligan, and M. A. Bourham, Phys. Fluids B **3**, 3046 (1991).
[19]K. Kim, IEEE Trans. Plasma Sci. **31**, 729 (2003).
[20]M. Keidar, J. Fan, I. D. Boyd, and I. I. Beilis, J. Appl. Phys. **89**, 3095 (2001).
[21]M. Keidar, I. D. Boyd, and I. I. Beilis, J. Phys. D **34**, 1675 (2001).
[22]M. Keidar, I. D. Boyd, and I. I. Beilis, J. Propul. Power **19**, 424 (2003).
[23]G. A. Bird, *Molecular Gas Dynamics and the Direct Simulation of Gas Flows* (Clarendon, Oxford, 1994).
[24]P. Kovatya and J. J. Lowke, J. Phys. D **17**, 1197 (1984).
[25]G. I. Kozlov, V. A. Kuznetsov, and V. A. Masyukov, Sov. Phys. JETP **39**, 463 (1974).
[26]A. I. Zemskov, V. V. Prut, and V. A. Khrabrov, Sov. Phys. Tech. Phys. **17**, 285 (1972).
[27]P. Kovatya, IEEE Trans. Plasma Sci. **12**, 38 (1984).
[28]C. S. Schmahl and P. J. Turchi, *Proceeding of the International Electric Propulsion Conference* (The Electric Propulsion Society, Worthington, OH, 1997), Vol. 1, p. 781.
[29]H. R. Griem, Phys. Rev. **128**, 997 (1962).
[30]K. Gunther and R. Radke, *Electrical Properties of Weakly Non-ideal Plasmas* (Boston, Birhauser, 1984).
[31]M. Keidar, I. D. Boyd, E. Antonsen, F. Gulchinski, and G. G. Spanjers, J. Propul. Power **20**, 978 (2004).
[32]H. Orbey, C. P. Bokis, and C. C. Chen, Ind. Eng. Chem. Res. **37**, 4481 (1998).
[33]C. F. Beaton and G. F. Hewitt, *Physical Property Data for Design Engineer* (Hemisphere, New York, 1989).
[34]R. A. Beyer and R. A. Pesce-Rodriguez, IEEE Trans. Magn. **39**, 207 (2003).
[35]M. J. Taylor, Propellants, Explos., Pyrotech. **26**, 137 (2001).